*Korean J. Chem. Eng.*, 38(3), 645-651 (2021)
DOI: 10.1007/s11814-020-0711-2

pISSN: 0256-1115
eISSN: 1975-7220

# Enhancing response time of micro-patterned thermoresponsive hydrogels by incorporation of pores

**Si-Eun Park and Seog-Jin Jeon†**

Department of Polymer Science and Engineering, Kumoh National Institute of Technology, Gumi, Gyeongbuk 39177, Korea
(*Received 27 August 2020 • Revised 19 October 2020 • Accepted 11 November 2020*)

**Abstract**−Micro-patterned hydrogels have received increasing attention in various research fields that need a fine structure and advanced functions compared to bulk hydrogels. For enhancing their performance, control of the size and distribution of pores in hydrogels is crucial. In particular, for the application of thermoresponsive hydrogels to a soft actuator, the characteristics of pores play an important role in enhancing the response time. We formed a porous structure in micro-patterns of polydiethylacrylamide (PDEAM), a thermoresponsive hydrogel, and analyzed the effect of pore size on the response time of the patterned hydrogels. Micro-patterned thermoresponsive hydrogels are fabricated by photo-crosslinking PDEAM copolymerized with benzophenone photo-crosslinker and polystyrene (PS) as a porogen. Pores sufficiently smaller than patterned objects, between a few micrometers to a few tens of micrometers, are successfully formed by controlling the content and molecular weight of PS. As the size and number of pores increase, the response time is improved, and the response time for swelling and deswelling is improved by up to 52 and 43% by blending PDEAM with 50 vol% of low molecular weight PS (5 kg/mol). This simple way to form a sub-millimeter scale hydrogel structure with controlled pores can be utilized in the emerging research fields, including 3D cell scaffolds, targeted drug delivery, and soft robotics.

Keywords: Porous Hydrogels, Micro-pattern, Thermoresponsive, Response Time

## INTRODUCTION

Micro-patterned hydrogels have received increasing attention due to emerging applications such as 3D cell scaffolds [1,2], targeted drug delivery [3], and soft robotics [4-6]. Compared to conventional cell scaffolds, micro-patterned scaffolds have an advantage in that they can control the spatial placement of cells and simultaneously control the three-dimensional structure of scaffolds, thereby promoting cell proliferation [7,8]. Micro-scale actuators are expected to expand the scope of non-invasive treatment by performing tasks such as controlled drug delivery or biopsy in the human body [9-11]. In these applications, control of pore size and distribution is important for enhancing their performance. Especially for micro-scale actuators, well-controlled pores can increase water penetration and diffusion rate, contributing to enhancing the response time of actuators [12-14].

For bulk hydrogels, many efforts have been made to introduce porous structures into hydrogels. The most popular method is the leaching of a porogen after crosslinking due to its simplicity [15-18]. As a porogen, polymer [15], sodium chloride [16], glucose [17], and silica [18] have been used to form pores ranging from several micrometers to hundreds of micrometers. In addition to the porogen method, there are other methods such as freeze-drying [19-21], mesophase templating [22], and electrospinning [23]. However, the methods other than the porogen method are too complicated to work in parallel with the micro-patterning method and, often, the pore size of interest is larger than the feature size of micro-patterned objects for the porogen method. Therefore, only a few studies have been conducted for micro-patterned porous hydrogels. Recently, Bryant et al. fabricated a porous poly(2-hydroxyethyl methacrylate) structure with a thickness of 700 μm having pores ranging from 62 to 147 μm using poly(methyl methacrylate) (PMMA) sphere porogen [24]. The process provides a wide range of controllable pore sizes, but the long dissolution time for PMMA (≈2 days) significantly reduces production efficiency. Wang et al. succeeded in forming a cylindrical hydrogel structure of several tens of micrometers in diameter with a pore size controlled from 400 nm to 4 μm by controlling the degree of phase separation of NaCl that occurs during photo-crosslinking of polyethylene glycol diacrylate [25]. Though the fine control of pore size is available, the single liquid phase forms only at low content of NaCl, which limits the formation of more dense pores. Therefore, it is necessary to develop a method that effectively facilitates pore formation and porosity control in micro-patterned hydrogels. Moreover, the formation of pores in micro-patterned stimuli-responsive hydrogels and regarding swelling behavior depending on their pore sizes is largely unexplored.

We formed porous micro-patterns of polydiethylacrylamide (PDEAM), a thermoresponsive hydrogel, which have pendent benzophenone (BP) photo-crosslinkers by introducing a suitable porogen. Among various porogens ranging from organic to inorganic, polymers are highly beneficial for the fabrication of porous hydrogels. Particularly advantageous is that the size of the pore can be controlled by molecular weight and content [26,27]. We employed polystyrene (PS) as a porogen based on the consideration of crosslinking efficiency by BP crosslinker in a previous result of Chris-

†To whom correspondence should be addressed.
E-mail: sjjeon@kumoh.ac.kr

tensen et al. [28]. The porous micro-patterned structures of stimuli-responsive hydrogels were successfully formed and the porosity was controlled by the molecular weight and content of the PS introduced. The porous structure showed up to 52% improvement in the response time in swelling kinetics. This result will contribute to improving the response time of soft micro-robots and developing tissue scaffolds or drug carriers with well-controlled pores.

## MATERIALS AND METHODS

### 1. Materials

$\alpha,\alpha'$-azobis(isobutyronitrile) (AIBN, Junsei), *N*,*N*-diethylacrylamide (DEAM, 98%, TCI), 4-aminobenzophenone (Aldrich), acryloyl chloride (TCI), dichloromethane (TCI), triethylamine (Aldrich), polystyrene (PS5K, MW 5,460, Polymer Laboratories), polystyrene (PS50K, MW 50,000, Pressure Chemical Co.), 1,4-dioxane (99.8%, anhydrous, Aldrich), poly(acrylic acid) (PAA, sodilum salt, 35% soln. in water, Polysciences), toluene (Daejung), hexane (Daejung), and acetone (99.5%, Daejung) were used as received.

### 2. Synthesis of PDEAM Copolymerized with BP

Polymers were synthesized by free-radical polymerization following procedures described previously [28]. Amounts of 3.24 mL of DEAM, 139 mg acrylamidobenzophenone, and 13 mg of AIBN were polymerized in 30 mL of 1,4-dioxane at 80 °C for 18 h under nitrogen, resulting in PDEAM copolymer with a benzophenone molar fraction of 0.023. AIBN was recrystallized from methanol prior to use. Acrylamidobenzophenone monomer was synthesized by the reaction of 4-aminobenzophenone with acryloyl chloride in dichloromethane and triethylamine [29]. The PDEAM copolymer was purified by precipitation into stirring hexane, washed by filtration, and dried in a vacuum oven overnight. The molecular weight of the PDEAM copolymer was 39 kg/mol, measured using GPC (Shimadzu Prominence). The composition of the PDEAM copolymer was verified by $^1$H NMR as shown in Fig. S1 (Bruker Avance III 400 MHz).

### 3. Formation of Porous Micro-patterns

We prepared 3 vol% solution of PDEAM, PS5K, PS50K, and 1 : 1 blend of PS5K and PS50K (MIX), respectively, in toluene. By mixing the solutions, three sets of 3 vol% blend solution of PS5K and PDEAM were prepared. Each solution contained 10, 30, and 50 vol% PS5K, and was designated as PS5K10, PS5K30, and PS5K50, respectively, for convenience. Two sets of blend solution of PS50K and PDEAM were prepared. Each solution contained 10 and 30 vol% PS50K and designated as PS50K10 and PS50K30. Two sets of blend solution of MIX and PDEAM, with each solution including 10 and 30 vol% MIX and designated as M10 and M30. The sample names and regarding the mixing ratio are summarized in Table 1. We used silicon ($S_i$) wafers as substrates for the deposition of the polymer solutions. Prior to deposition, the Si substrate was washed with water, acetone, and isopropanol for 10 min each in an ultrasonication bath and treated with UV-ozone to raise its surface energy. A thin layer of PAA crosslinked with $Ca^{2+}$ using $CaCl_2$ was coated on the Si substrate as a sacrificial layer before deposition. 25 μL of the polymer solutions were placed on the substrate and evaporated for 6 h at 60 °C in a nearly closed glass bottle, leading to a thickness of ≈3 μm. Due to the possible influence of the thickness on response time, the thickness of all samples was measured by a stylus profilometer (AlphaStep, Kla-tencor) and the variation was kept within 10%. Crosslinking was conducted using a UV light (365 nm, Solis-365, Thorlabs). Using a photomask, a circular pattern with a diameter of 180 μm was photo-patterned. Uncrosslinked polymers were developed using a 3 : 2 volume ratio solution of toluene and hexane.

**Table 1. The list of samples with swelling ratio and response time**

| Sample name | PS5K (vol%) | PS50K (vol%) | Swelling ratio | $t_s$ (sec) | $t_d$ (sec) |
|---|---|---|---|---|---|
| PDEAM | - | - | 1.83 | 450 | 170 |
| PS5K10 | 10 | - | 1.75 | 340 | 140 |
| PS5K30 | 30 | - | 1.67 | 300 | 100 |
| PS5K50 | 50 | - | 1.60 | 220 | 90 |
| PS50K10 | - | 10 | 1.68 | 280 | 110 |
| PS50K30 | - | 30 | 1.63 | 230 | 90 |
| M10 | 5 | 5 | 1.58 | 290 | 130 |
| M30 | 15 | 15 | 1.54 | 230 | 90 |

### 4. Response Time Measurement

The photo-patterned samples were released from the substrate using a buffered aqueous solution (pH 7.2 phosphate buffer; $1\times10^{-3}$ M NaCl) and observed using a Nikon LV100N uplight microscope with a 5x objective lens. A temperature stage (Linkam T95, LNP) with liquid nitrogen cooling was used for temperature control of the aqueous bath between 5 °C and 55 °C. The diameter of circular patterns of hydrogels was measured from images recorded at regular time intervals during the temperature change.

### 5. Characterization

For the observation of the pore size of samples, each sample was instantly frozen in the swollen state using liquid nitrogen and freeze-dried. The magnified images of the freeze-dried samples were taken using a field-emission scanning electron microscope (SEM, JEOL 6500F). To determine the average size of pores, at least 60 pores were analyzed from SEM images by the image analysis software (Image J).

## RESULTS AND DISCUSSION

We fabricated porous hydrogels using PDEAM copolymerized with BP, that has been used for the fabrication of various three-dimensional structures using micro-patterning of hydrogels [30-33]. Micro-patterned PDEAM is formed by photo-crosslinking of blend films of PDEAM and PS and subsequent removal of PS. Both polymers are soluble in toluene and form a homogeneous film, but show a significant difference in crosslinking efficiency with BP. BP shows high hydrogen abstraction efficiency for hydrogen atoms neighboring nitrogen of PDEAM, while PS has the least reactivity with BP [28]. Therefore, only PDEAM crosslinks and porous hydrogels are obtained after removing uncrosslinked PS.

For control of pore sizes, two different molecular weight PSs, PS5K or PS50K, or 1 : 1 mixture of them (MIX) were blended with PDEAM in various proportions. PS5K has a much smaller molecular weight than PDEAM (Mw=39 kg/mol), and PS50K has slightly

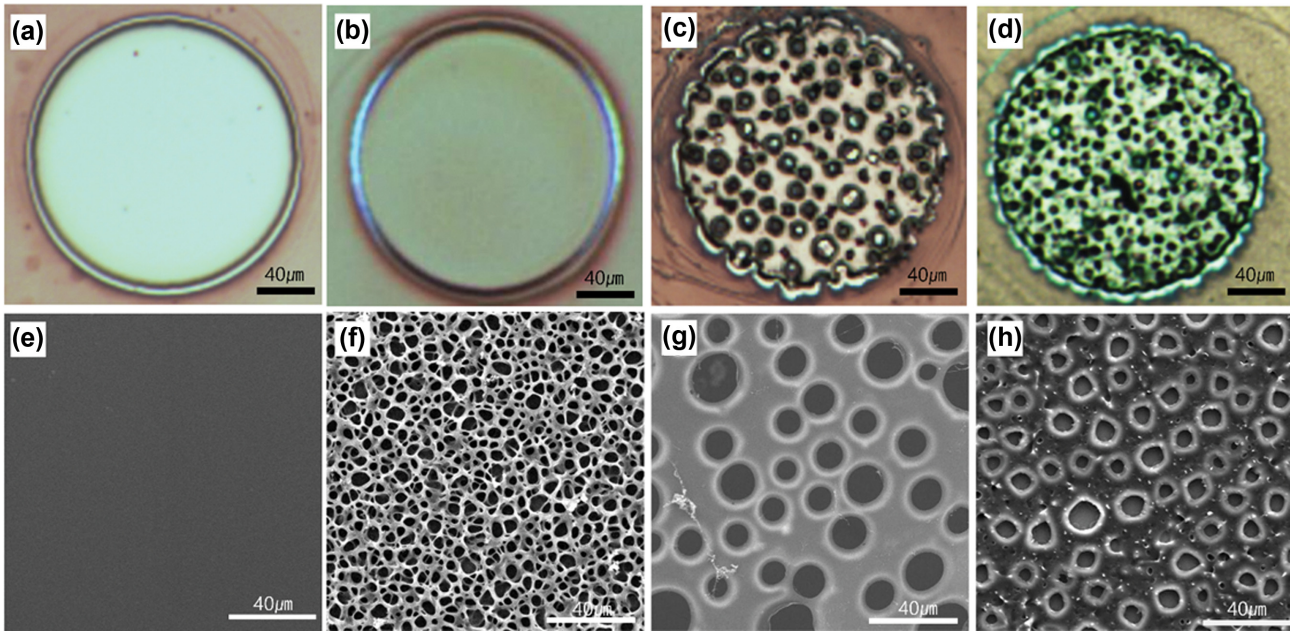


**Fig. 1. (a)-(d) Optical microscope images of circular micro-patterns of (a) PDEAM, (b) PS5K50, (c) PS50K30, and (d) M30 that are dried in air. (e)-(h) SEM images of (e) PDEAM, (f) PS5K50, (g) PS50K30, and (h) M30 that are instantly freeze-dried in a swelled state.**

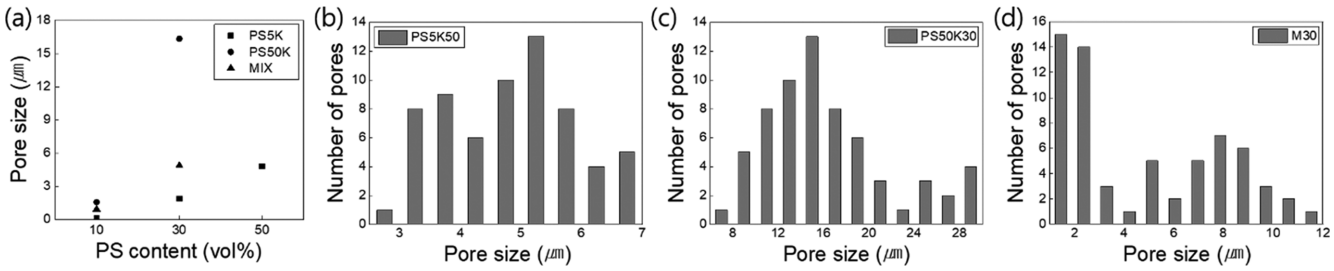


**Fig. 2. (a) Summary of the average pore size of porous hydrogels over PS content and (b)-(d) the pore size distribution of (b) PS5K50, (c) PS50K30, and (d) M30.**

higher molecular weight than PDEAM. The blend film was prepared using drop-casting and photo-patterned in a circle with a diameter of 180 μm. For PS5K, circular patterns are formed for PS content smaller than 50 vol% (Fig. 1(a)), but for the PS content larger than 60 vol%, patterns are collapsed because of the continuous phase transition from PDEAM to PS. For PS50K or MIX, circular patterns are formed for PS content smaller than 40 vol% (Fig. S2(a), (b)), but island-shape discontinuous domains appear for the PS content of 50 vol% (Fig. S2(c)). Thus, we kept the PS content lower than the critical PS content. For convenience, we use an abbreviation for each blended sample. For example, PS5K50 stands for the blend containing 50 vol% of PS5K, and M30 stands for the blend containing 30 vol% of MIX. PDEAM stands for PDEAM copolymer alone. The composition of samples is summarized in Table 1.

Optical microscope images of the resulting circular patterns in a dried state are shown in Fig. 1(a)-(d). Pores are not seen in PDEAM and PS5K50, while they are clearly seen in PS50K30 and M30. To observe the pores in the swelled state, we sufficiently swelled the samples at 5 °C and froze them instantly by immersing them in a Dewar filled with liquid nitrogen, followed by freeze-drying. While pores are not seen at the magnified SEM image of PDEAM (Fig. 1(e)), porous structures are clearly seen in SEM images of PS5K50, PS50K30, and MIX30 (Fig. 1(f)-(h)). We note that pores are not seen in PS5K50 in a deswelled or dried state (Fig. 1(b)), but they appear when it is instantly freeze-dried in a swelled state (Fig. 1(f)). Moreover, the pore size increase is observed for PS50K30 and M30 in their freeze-dried samples (Fig. 1(g), (h)) relative to dried samples (Fig. 1(c), (d)). We speculate that pores are collapsed or contracted in a deswelled or dried state, but they are restored during swelling.

For the blends containing lower molecular weight PS, the average pore sizes of freeze-dried samples for PS5K10, PS5K30, and PS5K50 are 0.11, 1.88, and 4.82 μm, respectively. For the blends containing higher molecular weight PS, the average pore sizes for PS50K10 and PS50K30 are 1.57 and 16.32 μm. For the blends containing MIX, the average pore sizes for M10 and M30 are 0.92 and 4.87 μm. Those average pore sizes are summarized in Fig. 2(a). In all cases, the size of pores increases monotonically with the increase in PS content. Furthermore, the blends containing higher

molecular weight PS show larger pore sizes due to the nature of the higher molecular weight PS being segregated from PDEAM [26,27]. For example, for 30% of PS, the average pore size of PS50K30 is 8.7-times that of PS5K30. The pore size distribution of PS5K30 and PS50K30 is close to monodisperse (Fig. 2(b), (c)), while that of M30 is bidisperse due to the contribution of the two different molecular weight PSs (Fig. 2(d)).

Next, we observe the thermoresponsive swelling behavior of the porous samples. The swelling ratio ($\chi_i$) is defined as Eq. (1).

$$\chi_i = \frac{D}{D_0} \tag{1}$$

All samples are photo-patterned in a circle, and their diameters, D and $D_0$, are measured from microscope images. $D_0$ is a diameter of the deswelled sample at 55 °C, and D is a diameter of the swelled sample at 5 °C. PDEAM shows the largest swelling ratio, 1.83, and the swelling ratio decreases as the content of PS increases (Table 1), because the swellable PDEAM is replaced with non-swellable pores. If we calculate the expected swelling ratio based on the volume of PDEAM replaced, it is 1.75, 1.66, and 1.58 for 10, 30, and 50 vol% replacement, respectively, which shows good agreement with the measured swelling ratio of PS5K10, PS5K30, and PS5K50 (Fig. S3). This result proves leach out of PS5K from the blends. The slightly larger values of measurement than the calculation for PS5K samples are considered the measurement error due to the transparent hydrogel's unclear edge boundary. Additionally, we confirmed the removal of PS by Raman spectroscopy (Fig. 3). PS has a sharp characteristic peak at 1,000 $cm^{-1}$ assigned to ring breathing mode (Fig. 3(a)). The peak observed at a Raman shift slightly lower than 1,000 $cm^{-1}$ in Fig. 3(a)-(c) is for a silicon substrate. The Raman spectrum of PDEAM shows peaks at 1,455 and 1,620 $cm^{-1}$, characteristic peaks of PDEAM, and a very weak peak at 860 $cm^{-1}$ for para-disubstituted benzene of benzophenone due to its low content, 2.3 mol% (Fig. 3(b)). For PS5K50, the PS characteristic peak at 1,000 $cm^{-1}$ disappeared (Fig. 3(c)), and the spectrum is almost the same as that of PDEAM (Fig. 3(b)), which confirms the removal of PS. In the case of PS50K and MIX, the measured swelling ratio is much smaller than the expected swelling ratio (Fig. S3). We speculate that the crosslinking of PDEAM is significantly interrupted by the higher molecular weight PS, and thus a significant amount of uncrosslinked PDEAM is removed by development. We normalized the swelling ratio using Eq. (2) for comparison, and all plots of swelling ratio against time are prepared based on the normalized swelling ratio, $Z_i$ (Figs. 4 and 5).

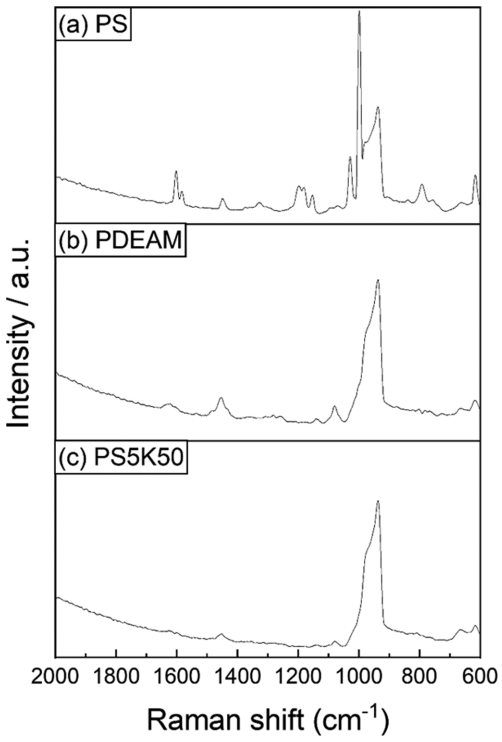


**Fig. 3. Raman spectra of (a) PS, (b) PDEAM, and (c) PS5K50.**

$$Z_i = \frac{x_i - \min(x)}{\max(x) - \min(x)} \tag{2}$$

$x_i$ is the swelling ratio at the time $t_i$. max(x) and min(x) are the largest and the smallest swelling ratio of all $x_i$.

We first performed the swelling experiment. The samples were fully deswelled at 55 °C for at least 10 min, and the temperature was rapidly decreased to 5 °C for swelling. For the calculation of the swelling response time, $t_s$, we defined $t_v$ and $t_f$. $t_v$ is defined as the time it takes for the temperature to reach the volume phase transition temperature (VPTT) of PDEAM, 32 °C. $t_v$ is determined by the time showing the steepest change in swelling in the swelling ratio vs. time graph [34,35], and denoted with arrows in Fig. 4(a)-(c). $t_f$ is defined as the time it takes for the sample to reach the maximum swelling ratio. Then, we compared $t_s$, defined by Eq. (3).

$$t_s \text{ (or } t_d) = t_f - t_v \tag{3}$$

For easier comparison of $t_s$, we exhibit $t - t_v$ vs. $Z_i$ curves in Fig. 4(d)-(f). PDEAM shows a long tail of a sluggish increase in swelling ratio after the sharp increase (Fig. 4(a)), resulting in $t_s$ of 460 sec (Fig. 4(d)). For the blends with PS5K, $t_s$ decreases as the content of PS increases (Fig. 4(d)). $t_s$ observed for PS5K10, PS5K30, and PS5K50 was 340, 290, and 220 sec, respectively, which corresponds to 26, 41, and 52% reduction in response time. For exact comparison in the $t_s$, the enlarged plot is shown in inset of Fig. 4(d). For the blend with the higher molecular weight PS, $t_s$ observed for PS50K10 and PS50K30 is 280 and 230 sec, corresponding to 39 and 50% reduction in response time (Fig. 4(e)). The $t_s$ comparison of PS5K30 and PS50K30 shows that larger pores are more effective for enhancing response time. From the additional experiments for the blend of PDEAM with MIX, $t_s$ observed for M10 and M30 is 300 and 230 sec, which corresponds to 35 and 50% reduction in response time (Fig. 4(f)). Though the average pore size of M30 is smaller than PS50K30, the reduction in response time is the same. This phenomenon is probably due to the synergistic effect of increased proximity between smaller pores and enhanced water transport capacity of larger pores. Among all samples, PS5K50 exhibits the highest reduction in response time. Considering that the size of PS5K50 is only one-ninth of PS50K30, this high enhancement is noticeable. We speculate that the remarkable enhancement is caused by the high density of pores and the interconnected pore network. In Fig. 1(f), the large contact area between

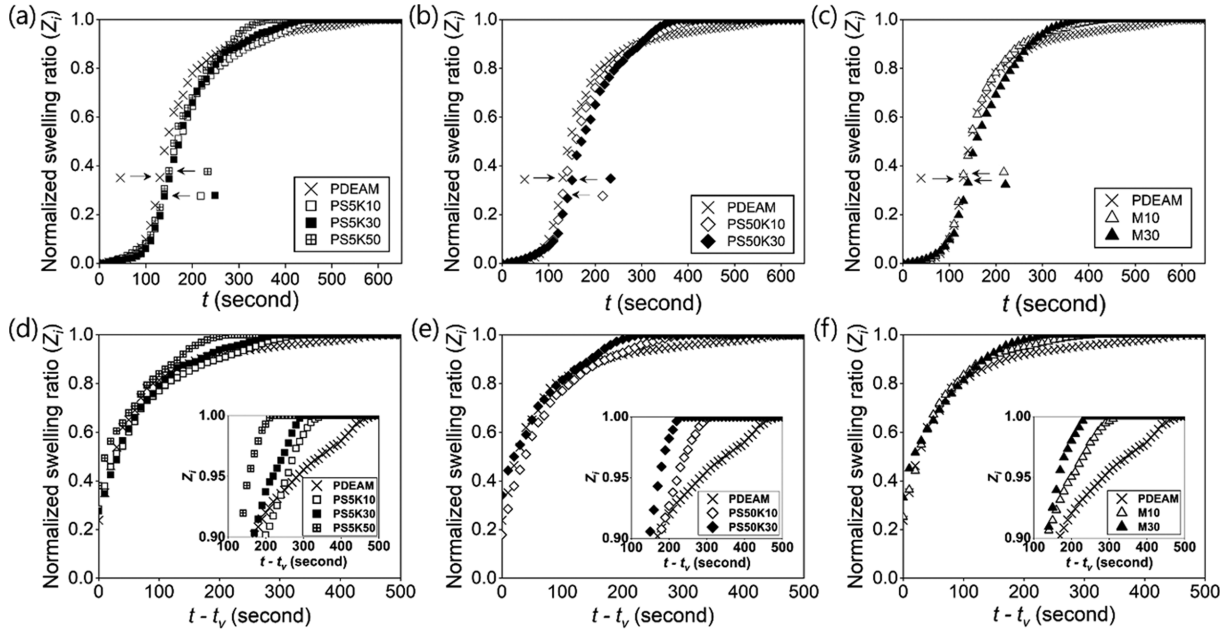


**Fig. 4. Plots of the normalized swelling ratio ($Z_i$) over time for swelling experiments. (a)-(c) $Z_i$ vs. t curves for (a) PS5K, (b) PS50K, and (c) MIX for the start of cooling at t=0. Arrows are indicating the location of $t_v$. (d)-(f) $Z_i$ vs. $t-t_v$ curves for (d) PS5K, (e) PS50K, and (f) MIX. Insets are enlarged curves.**

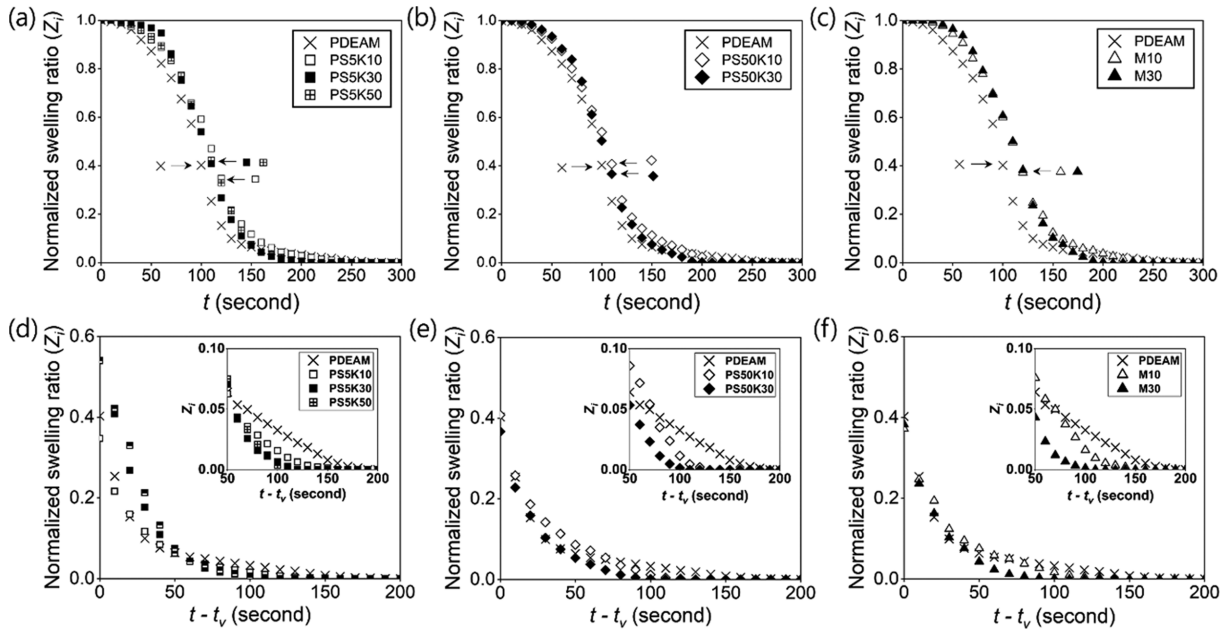


**Fig. 5. Plots of the normalized swelling ratio ($Z_i$) over time for deswelling experiments. (a)-(c) $Z_i$ vs. t curves for (a) PS5K, (b) PS50K, and (c) MIX for the start of heating at t=0. Arrows are indicating the location of $t_v$. (d)-(f) $Z_i$ vs. $t-t_v$ curves for (d) PS5K, (e) PS50K, and (f) MIX. Insets are enlarged curves.**

hydrogel and water by the high pore density allows efficient water diffusion. The interconnected pore network is expected to promote the rapid movement of water molecules inside the hydrogel.

Next, we turn to the deswelling experiment. The samples were fully swelled at 5 °C for at least 10 min, and the temperature was rapidly increased to 55 °C for the deswelling. We compared $t_d$, defined by the time it takes for the deswelling reaches its final state after $t_v$. The location of $t_v$ that shows the steepest change in the curves is denoted by arrows in Fig. 5(a)-(c), and $t-t_v$ vs. $Z_i$ are shown in Fig. 5(d)-(f). All samples show faster response than swelling experiments, and PDEAM shows the slowest response, as shown in Fig. 5(d) ($t_d$=185 sec). For the blends with the low molecular weight PS, $t_d$ for PS5K10, PS5K30, and PS5K50 is 155, 115, and 105 sec (Fig. 5(d)), respectively. For the blends with the high molecu-

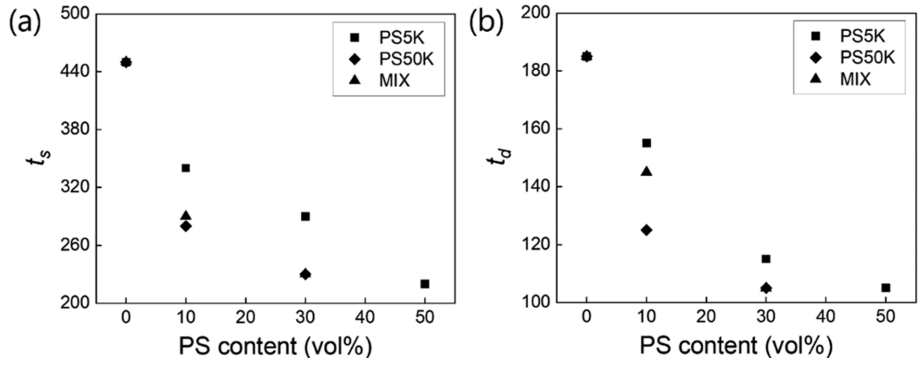


**Fig. 6. (a) Summary of $t_s$ and (b) $t_d$ according to PS content.**

lar weight PS, $t_d$ for PS50K10 and PS50K30 is 125 and 105 sec (Fig. 5(e)). Finally, for the blends with MIX, $t_d$ for M10 and M30 is 145 and 105 sec (Fig. 5(f)). The highest reduction in response time, 43%, is observed for PS5K50, PS50K30, and M30.

We summarize $t_s$ and $t_d$ for all samples in Fig. 6. The highest enhancement in response time is observed for PS5K50, 52 and 43% reduction for swelling and deswelling. We believe that such an enhancement will also be possible for other stimuli-responsive hydrogels, including poly(*N*-isopropyl acrylamide), due to the square dependence of response time on hydrogels' average diffusion path length [12-14]. Though significant enhancement in response time is observed, further improvement is expected by introducing a more efficient way to change the temperature. According to the temperature profile of aqueous bath vs. time for swelling experiment (Fig. S4), it takes about 500 sec to reach the set temperature, 5 °C, even though liquid nitrogen cooling is used. Thus, there is much room for further improvement in response time by employing more efficient methods for temperature change, e.g., photothermal heating [36,37]. Besides the response time, durability is essential for various applications. Though the increase in porosity causes a reduction in the mechanical strength of hydrogels, we expect that various reinforcing approaches developed so far can compensate for the reduced mechanical strength. Our pore formation approach can easily be accompanied by reinforcing approaches based on nanocomposite formation [38,39], interpenetrating polymer network [40,41], and hydrogel hybrids with rigid elements [4], due to its simplicity. With the combinatorial approach, we expect the implementation of durable and fast responsive hydrogels.

## CONCLUSION

We have successfully fabricated micro-patterned porous hydrogels with controlled pore sizes from hundreds of nanometers to a few tens of micrometers by selecting a suitable porogen, PS. Two different molecular weight PSs, PS5K or PS50K, or 1 : 1 mixture of them, have been blended with PDEAM and removed by development after photo-crosslinking of PDEAM, which resulted in the formation of porous PDEAM. Higher molecular weight or higher content of PS causes a larger pore size; the largest and smallest average pore sizes obtained were 0.11 and 16.3 μm for PS5K10 and PS50K30, respectively. Response time decreased as the pore size increased, and the formation of larger pore played a more dominant role in the reduction in response time. However, the higher molecular weight PS, which resulted in larger pores, disrupted photo-crosslinking of PDEAM and their blends showed reduced swelling ratio. The most substantial reduction in response time, 52% and 43%, was observed for swelling and deswelling of PS5K50 due to the proximity between pores. This research provides a simple way to form pores in the photo-patterned stimuli-responsive hydrogel and is potentially applicable to developing novel 3D cell scaffolds, targeted drug carriers, and micro-robots.

## ACKNOWLEDGEMENT

This work was supported by Kumoh National Institute of Technology (2018-104-145).

## NOTES

The authors declare no competing financial interest.

## SUPPORTING INFORMATION

Additional information as noted in the text. This information is available via the Internet at http://www.springer.com/chemistry/journal/11814.

## REFERENCES

1. J. L. Ifkovits and J. A. Burdick, *Tissue Eng.*, **13**, 2369 (2007).
2. R. F. Pereira and P. J. Bártolo, *Engineering*, **1**, 90 (2015).
3. J. Li and D. J. Mooney, *Nat. Rev. Mater.*, **1**, 16071 (2016).
4. S.-J. Jeon, A. W. Hauser and R. C. Hayward, *Acc. Chem. Res.*, **50**, 161 (2017).
5. T. van Manen, S. Janbaz and A. A. Zadpoor, *Mater. Today*, **21**, 144 (2018).
6. O. Erol, A. Pantula, W. Liu and D. H. Gracias, *Adv. Mater. Technol.*, **4**, 1900043 (2019).
7. B. M. Baker and C. S. Chen, *J. Cell Sci.*, **125**, 3015 (2012).
8. M. Jamal, S. S. Kadam, R. Xiao, F. Jivan, T.-M. Onn, R. Fernandes, T. D. Nguyen and D. H. Gracias, *Adv. Healthcare Mater.*, **2**, 1142 (2013).

9. T. S. Shim, S.-H. Kim, C.-J. Heo, H. C. Jeon and S.-M. Yang, *Angew. Chem. Int. Ed.*, **51**, 1420 (2012).
10. T. G. Leong, C. L. Randall, B. R. Benson, N. Bassik, G. M. Stern and D. H. Gracias, *Proc. Natl. Acad. Sci. U.S.A.*, **106**, 703 (2009).
11. M. Cianchetti, C. Laschi, A. Menciassi and P. Dario, *Nat. Rev. Mater.*, **3**, 143 (2018).
12. T. Tanaka and D. J. Fillmore, *J. Chem. Phys.*, **70**, 1214 (1970).
13. M. Shibayama and T. Tanaka, *Adv. Polym. Sci.*, **109**, 1 (1993).
14. X.-Z. Zhang, X.-D. Xu, S.-X. Cheng and R.-X. Zhuo, *Soft Matter*, **4**, 385 (2008).
15. X.-Z. Zhang, Y.-Y. Yang, T.-S. Chung and K.-X. Ma, *Langmuir*, **17**, 6094 (2001).
16. S.-X. Cheng, J.-T. Zhang and R.-X. Zhuo, *J. Biomed. Mater. Res. A*, **67**, 96 (2003).
17. J.-T. Zhang, S.-X. Cheng and R.-X. Zhuo, *J. Polym. Sci., Part A: Polym. Chem.*, **41**, 2390 (2003).
18. T. Serizawa, K. Wakita and M. Akashi, *Macromolecules*, **35**, 10 (2002).
19. W. Xue, S. Champ, M. B. Huglin and T. G. J. Jones, *Eur. Polym. J.*, **40**, 467 (2004).
20. J. Grenier, H. Duval, F. Barou, P. Lv, B. David and D. Letourneur, *Acta Biomater.*, **94**, 195 (2019).
21. I. N. Savina, G. C. Ingavle, A. B. Cundy and S. V. Mikhalovsky, *Sci. Rep.*, **6**, 21154 (2016).
22. M. Antonietti, R. A. Caruso, C. G. Göltner and M. C. Weissenberger, *Macromolecules*, **32**, 1383 (1999).
23. S. Jiang, F. Liu, A. Lerch, L. Ionov and S. Argawal, *Adv. Mater.*, **27**, 4865 (2015).
24. S. J. Bryant, J. L. Cuy, K. D. Hauch and B. D. Ratner, *Biomaterials*, **28**, 2978 (2007).
25. S. Wang, L. Li, D. Su, K. Robin and K. A. Brown, *ACS Appl. Mater. Interfaces*, **10**, 34604 (2018).
26. J. S. Higgins, J. E. G. Lipson and R. P. White, *Phil. Trans. R. Soc. A*, **368**, 1009 (2010).
27. S. Walheim, M. Böltau, J. Mlynek, G. Krausch and U. Steiner, *Macromolecules*, **30**, 4995 (1997).
28. S. K. Christensen, M. C. Chiappelli and R. C. Hayward, *Macromolecules*, **45**, 5237 (2012).
29. J. Jia, M. Sarker, M. G. Steinmetz, R. Shukla and R. J. Rathore, *J. Org. Chem.*, **73**, 8867 (2008).
30. J. Kim, J. A. Hanna, M. Byun, C. D. Santangelo and R. C. Hayward, *Science*, **335**, 1201 (2012).
31. J. H. Na, A. A. Evans, J. Bae, M. C. Chiappelli, C. D. Santangelo, R. J. Lang, T. C. Hull and R. C. Hayward, *Adv. Mater.*, **27**, 79 (2015).
32. S.-J. Jeon and R. C. Hayward, *Adv. Mater.*, **29**, 1606111 (2017).
33. S.-J. Jeon and R. C. Hayward, *Soft Matter*, **16**, 688 (2020).
34. H. Kojima, *Polym. J.*, **50**, 411 (2018).
35. S. Bandyopadhyay, A. Sharma, M. A. A. Alvi, R. Raju and W. R. Glomm, *RSC Adv.*, **7**, 53192 (2017).
36. H. Guo, J. Cheng, J. Wang, P. Huang, Y. Liu, Z. Jia, X. Chen, K. Sui, T. Li and Z. Nie, *J. Mater. Chem. B*, **5**, 2883 (2017).
37. B. Ziółkowski, L. Florea, J. Theobald, F. Benito-Lopez and D. Diamond, *J. Mater. Sci.*, **51**, 1392 (2016).
38. J. Yi, G. Choe, J. Park and J. Y. Lee, *Polym. J.*, **52**, 823 (2020).
39. L. E. Beckett, J. T. Lewis, T. K. Tonge and L. T. J. Korley, *ACS Biomater. Sci. Eng.*, **6**, 5453 (2020).
40. E. C. Dragan, *Chem. Eng. J.*, **243**, 572 (2014).
41. J. P. Gong, *Soft Matter*, **6**, 2583 (2010).

# Supporting Information

# Enhancing response time of micro-patterned thermoresponsive hydrogels by incorporation of pores

**Si-Eun Park and Seog-Jin Jeon**†

Department of Polymer Science and Engineering, Kumoh National Institute of Technology, Gumi, Gyeongbuk 39177, Korea
(*Received 27 August 2020 • Revised 19 October 2020 • Accepted 11 November 2020*)

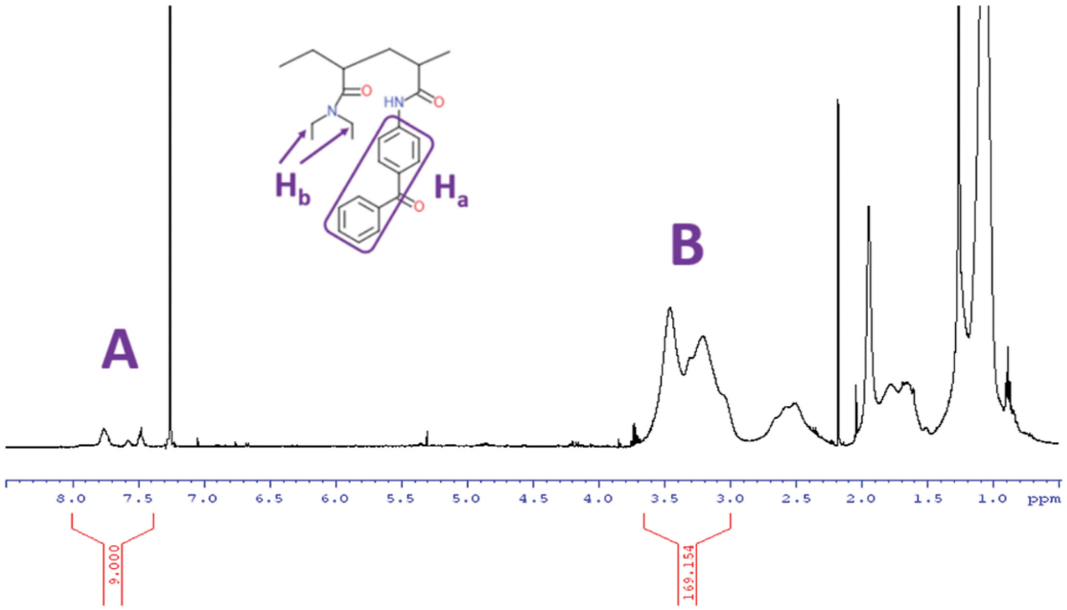


**Fig. S1.** $^1$H NMR spectra of PDEAM copolymerized with 2.3 mol% BP.

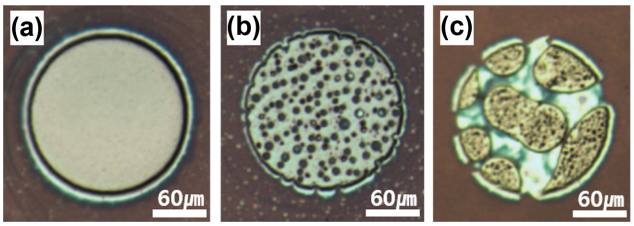


**Fig. S2.** Optical microscope images of (a) M10, (b) M30, and (c) M50.

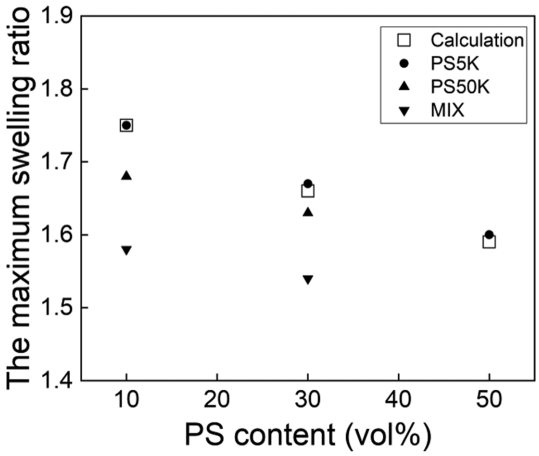


**Fig. S3.** The maximum swelling ratio according to the content of PS5K, PS50K, and MIX.

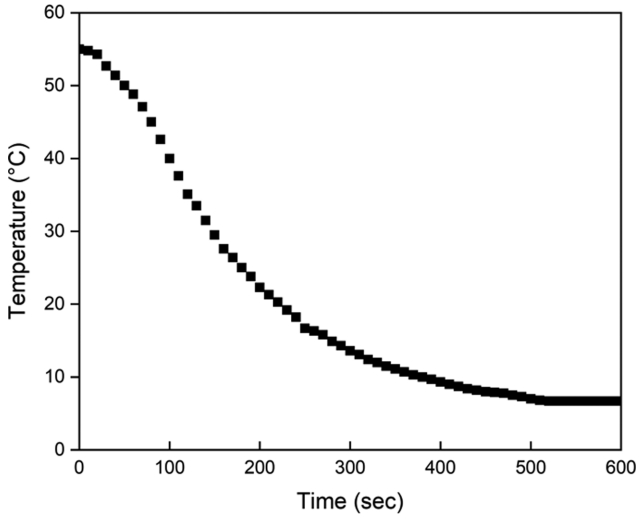


**Fig. S4. Temperature vs. time curve measured in the aqueous bath using a probe-type thermometer for swelling and deswelling.**